Variable Very-High-Energy Gamma-Ray Emission from the Microquasar LS I +61 303

J. Albert,[1] E. Aliu,[2] H. Anderhub,[3] P. Antoranz,[4] A. Armada,[2] M. Asensio,[4] C. Baixeras,[5] J. A. Barrio,[4] M. Bartelt,[6] H. Bartko,[7] D. Bastieri,[8] S. R. Bavikadi,[9] W. Bednarek,[10] K. Berger,[1] C. Bigongiari,[8] A. Biland,[3] E. Bisesi,[9] R. K. Bock,[7] P. Bordas,[11] V. Bosch-Ramon,[11] T. Bretz,[1] I. Britvitch,[3] M. Camara,[4] E. Carmona,[7] A. Chilingarian,[12] S. Ciprini,[13] J. A. Coarasa,[7] S. Commichau,[3] J. L. Contreras,[4] J. Cortina,[2] V. Curtef,[6] V. Danielyan,[12] F. Dazzi,[8] A. De Angelis,[9] R. de los Reyes,[4] B. De Lotto,[9] E. Domingo-Santamaría,[2] D. Dorner,[1] M. Doro,[8] M. Errando,[2] M. Fagiolini,[14] D. Ferenc,[15] E. Fernández,[2] R. Firpo,[2] J. Flix,[2] M. V. Fonseca,[4] L. Font,[5] M. Fuchs,[7] N. Galante,[14] M. Garczarczyk,[7] M. Gaug,[8] M. Giller,[10] F. Goebel,[7] D. Hakobyan,[12] M. Hayashida,[7] T. Hengstebeck,[16] D. Höhne,[1] J. Hose,[7] C. C. Hsu,[7] P. G. Isar,[7] P. Jacon,[10] O. Kalekin,[16] R. Kosyra,[7] D. Kranich,[3,15] M. Laatiaoui,[7] A. Laille,[15] T. Lenisa,[9] P. Liebing,[7] E. Lindfors,[13] S. Lombardi,[8] F. Longo,[17] J. López,[2] M. López,[4] E. Lorenz,[3,7] F. Lucarelli,[4] P. Majumdar,[7] G. Maneva,[18] K. Mannheim,[1] O. Mansutti,[9] M. Mariotti,[8] M. Martínez,[2] K. Mase,[7] D. Mazin,[7] C. Merck,[7] M. Meucci,[14] M. Meyer,[1] J. M. Miranda,[4] R. Mirzoyan,[7] S. Mizobuchi,[7] A. Moralejo,[2] K. Nilsson,[13] E. Oña-Wilhelmi,[2] R. Orduña,[5] N. Otte,[7] I. Oya,[4] D. Paneque,[7] R. Paoletti,[14] J. M. Paredes,[11] M. Pasanen,[13] D. Pascoli,[8] F. Pauss,[3] N. Pavel,[16*] R. Pegna,[14] M. Persic,[19] L. Peruzzo,[8] A. Piccioli,[14] M. Poller,[1] G. Pooley,[20] E. Prandini,[8] A. Raymers,[12] W. Rhode,[6] M. Ribó,[11] J. Rico,[2]† B. Riegel,[1] M. Rissi,[3] A. Robert,[5] G. E. Romero,[21,22] S. Rügamer,[1] A. Saggion,[8] A. Sánchez,[5] P. Sartori,[8] V. Scalzotto,[8] V. Scapin,[8] R. Schmitt,[1] T. Schweizer,[16] M. Shayduk,[16] K. Shinozaki,[7] S. N. Shore,[23] N. Sidro,[2]† A. Sillanpää,[13] D. Sobczynska,[10] A. Stamerra,[14] L. S. Stark,[3] L. Takalo,[13] P. Temnikov,[18] D. Tescaro,[2] M. Teshima,[7] N. Tonello,[7] A. Torres,[5] D. F. Torres,[2,24] N. Turini,[14] H. Vankov,[18] V. Vitale,[9] R. M. Wagner,[7] T. Wibig,[10] W. Wittek,[7] R. Zanin,[8] J. Zapatero[5]

Microquasars are binary star systems with relativistic radio-emitting jets. They are potential sources of cosmic rays and can be used to elucidate the physics of relativistic jets. We report the detection of variable gamma-ray emission above 100 gigaelectron volts from the microquasar LS I +61 303. Six orbital cycles were recorded. Several detections occur at a similar orbital phase, which suggests that the emission is periodic. The strongest gamma-ray emission is not observed when the two stars are closest to one another, implying a strong orbital modulation of the emission or absorption processes.

Microquasars are binary star systems consisting of a compact object of a few solar masses (either a neutron star or a black hole) and a companion star that loses mass into an accretion disk around the compact object. The most relevant feature of microquasars is that they display relativistic jets—outflows of matter from regions close to accreting black holes and neutron stars. These jets are among the most spectacular astrophysical phenomena, yet they remain poorly explained (*1*). In microquasars, the time scales of relevant processes, because they are correlated with the compact object's mass, are shorter than those in quasars by more than six orders of magnitude, allowing the study of a different range of variability. In addition, microquasars could measurably contribute to the density of galactic cosmic rays (*2*). It is noteworthy that photons up to very high energy (VHE) are an expected by-product of cosmic ray production.

Two GeV sources detected by the Energetic Gamma-Ray Experiment Telescope (EGRET) (*3*) are positionally compatible with microquasars. One of these, LS 5039 (*4*) in the Southern Hemisphere, was recently confirmed as a TeV emitter (*5*) by the High Energy Stereoscopic System (HESS). The other, LS I +61 303 (*6*), can be observed from the Northern Hemisphere and was thus a natural target for the Major Atmospheric Gamma-ray Imaging Cherenkov (MAGIC) telescope.

LS I +61 303 is a B0 main-sequence star with a circumstellar disc (i.e., a Be star) located at a distance of ~2 kpc (*7*). A compact object of unknown mass is orbiting around it every 26.496 days (*8*, *9*). The eccentricity of the orbit is 0.72 ± 0.15, and the periastron passage (the point where the two stars are closest to one another) is at phase 0.23 ± 0.02. The nature of the compact object is still debated (*10*). Radio outbursts are observed every orbital cycle from this system (*11*) at phases varying between 0.45 and 0.95 (*12*) with a modulation of 4.6 years. The monitoring of LS I +61 303 at x-ray energies (*13*–*15*) revealed x-ray outbursts starting around phase 0.4 and lasting up to phase 0.6. The detection of extended jetlike and likely rapidly precessing radio-emitting structures at angular extensions of 0.01 to 0.05 arc sec has been interpreted as unambiguous evidence of the microquasar nature of LS I +61 303 (*16*, *17*).

The gamma-ray source 3EG J0241+6103 (also known as 2CG 135+01) was discovered by Cosmic Ray Satellite B (COS-B) at energies above 100 MeV (*18*). Despite its large uncertainty (~1°) in position, the source was proposed to be the high-energy counterpart of the 26.5-day periodic radio outburst source GT 0236+610, which turned out to be the early-type star LS I +61 303 (*11*). The large uncertainty of the position of 3EG J0241+6103 did not allow unambiguous association with LS I +61 303. The GeV gamma-ray emission from this EGRET source is clearly variable (*19*). Even though the GeV data remain scarce in this regime, an increased emission has been suggested for the periastron passage (*20*) and was firmly reported around phase 0.5 (*6*), coincident with the x-ray outbursts.

MAGIC, located on La Palma, Canary Islands (Spain), is an imaging air Cherenkov telescope (IACT). This kind of instrument images the Cherenkov light produced in the particle cascade initiated by a gamma ray in the atmosphere. MAGIC (*21*, *22*) includes several innovative techniques and technologies in its design and is currently the largest single-dish telescope (diameter 17 m) in this energy band. It is equipped with a 576-pixel photomultiplier camera with a 3.5° field of view. The telescope's sensitivity above 100 GeV is ~2.5% of the Crab Nebula flux (the calibration standard candle for IACTs) in 50 hours of observations. The angular resolution is ~0.1°, and the energy

[1]Universität Würzburg, D-97074 Würzburg, Germany. [2]Institut de Física d'Altes Energies, E-08193 Bellaterra (Barcelona), Spain. [3]Eidgenössische Technische Hochschule Zürich, CH-8093 Zürich, Switzerland. [4]Universidad Complutense, E-28040 Madrid, Spain. [5]Universitat Autónoma de Barcelona, E-08193 Bellaterra, Spain. [6]Universität Dortmund, D-44227 Dortmund, Germany. [7]Max-Planck-Institut für Physik, D-80805 München, Germany. [8]Università di Padova and Istituto Nazionale di Fisica Nucleare (INFN), I-35131 Padova, Italy. [9]Università di Udine and INFN Trieste, I-33100 Udine, Italy. [10]University of Lodz, PL-90236 Lodz, Poland. [11]Universitat de Barcelona, E-08028 Barcelona, Spain. [12]Yerevan Physics Institute, 375036 Yerevan, Armenia. [13]Tuorla Observatory, FI-21500 Piikkiö, Finland. [14]Università di Siena and INFN Pisa, I-53100 Siena, Italy. [15]University of California, Davis, CA 95616, USA. [16]Humboldt-Universität zu Berlin, D-12489 Berlin, Germany. [17]Università di Trieste and INFN Trieste, I-34100 Trieste, Italy. [18]Institute for Nuclear Research and Nuclear Energy, BG-1784 Sofia, Bulgaria. [19]Osservatorio Astronomico and INFN Trieste, I-34100 Trieste, Italy. [20]Cavendish Laboratory, University of Cambridge, Cambridge CB3 0HE, UK. [21]Facultad de Ciencias Astronómicas y Geofísicas, UNLP, 1900 La Plata, Argentina. [22]Instituto Argentino de Radioastronomía CC5, 1894 Villa Elisa, Argentina. [23]Università di Pisa and INFN Pisa, I-56100 Pisa, Italy. [24]Institut de Ciències de l'Espai/Consejo Superior de Investigaciones Cientificas, E-08193 Bellaterra (Barcelona), Spain.

*Deceased.

†To whom correspondence should be addressed. E-mail: nsidro@ifae.es (N.S.); jrico@ifae.es (J.R.)

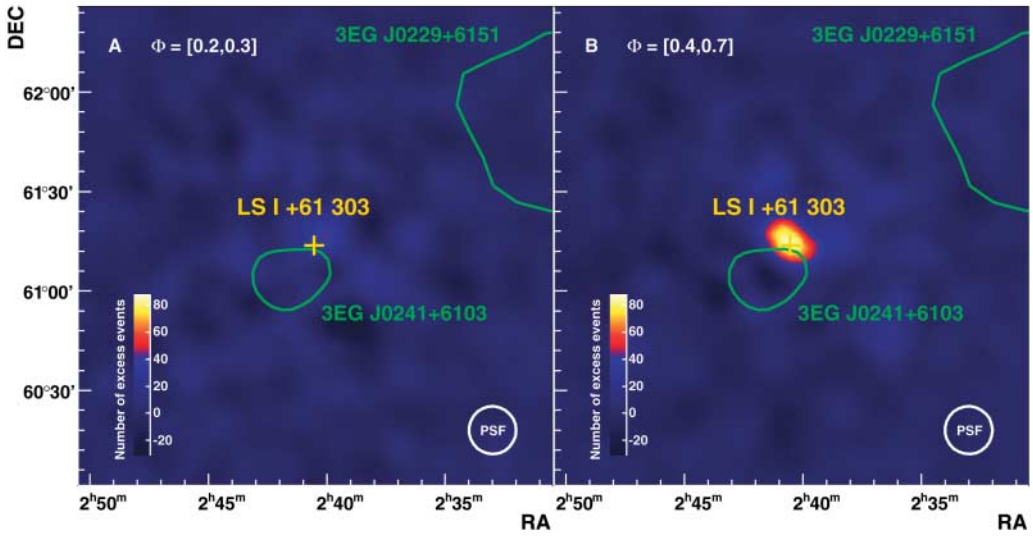

Fig. 1. Smoothed maps of gamma-ray excess events above 400 GeV around LS I +61 303. (**A**) Observations over 15.5 hours corresponding to data around periastron (i.e., between orbital phases 0.2 and 0.3). (**B**) Observations over 10.7 hours at orbital phase between 0.4 and 0.7. The number of events is normalized in both cases to 10.7 hours of observation. The position of the optical source LSI +61 303 (yellow cross) and the 95% confidence level contours for 3EG J0229+6151 and 3EG J0241+6103 (green contours) are also shown. The bottom right circle shows the size of the point spread function of MAGIC (1σ radius). No significant excess in the number of gamma-ray events is detected around periastron passage, whereas it shows up clearly (9.4σ statistical significance) at later orbital phases, in the location of LS I +61 303.

resolution above 200 GeV is better than 30%. MAGIC can provide gamma-ray source localization in the sky with a precision of ~2′.

LS I +61 303 was observed during 54 hours (after standard quality selection, discarding bad-weather data) between October 2005 and March 2006. MAGIC is unique among IACTs in its capability to operate in the presence of the Moon. This allows the duty cycle to be increased by up to 50%, thus considerably improving the sampling of variable sources. In particular, 22% of the data used in this analysis were recorded under moonlight. The data analysis was carried out using the standard MAGIC analysis and reconstruction software (*21*, *22*).

The reconstructed gamma-ray map (Fig. 1) during two different observation periods, around periastron passage and at higher (0.4 to 0.7) orbital phases, clearly shows an excess in the latter case. The excess is located at (J2000) $\alpha = 2^h40^m34^s$, $\delta = 61°15'25''$, with statistical and systematic uncertainties of ±0.4′ and ±2′, respectively, in agreement with the position of LS I +61 303. The distribution of gamma-ray excess is consistent with a pointlike source. In the natural case in which the VHE emission is produced by the same object detected at EGRET energies, this result identifies a gamma-ray source that resisted classification during the past three decades.

Our measurements show that the VHE gamma-ray emission from LS I +61 303 is variable. The gamma-ray flux above 400 GeV coming from the direction of LS I +61 303 (Fig. 2) has a maximum corresponding to ~16% of the Crab Nebula flux and is detected around phase 0.6. The combined statistical significance of the three highest flux measurements is 8.7σ, for an integrated observation time of 4.2 hours. The probability for the distribution of measured fluxes to be a statistical fluctuation of a constant flux (obtained from a χ^2 fit of a constant function to the entire data sample) is 3×10^{-5}. The fact that the detections occur at similar orbital phases suggests a periodic nature of the VHE gamma-ray emission. Contemporaneous radio observations of LS I +61 303 were carried out at 15 GHz with the Ryle Telescope covering several orbital periods of the source. The peak of the radio outbursts was at phase 0.7, just after the increase of the VHE gamma-ray flux (fig. S1).

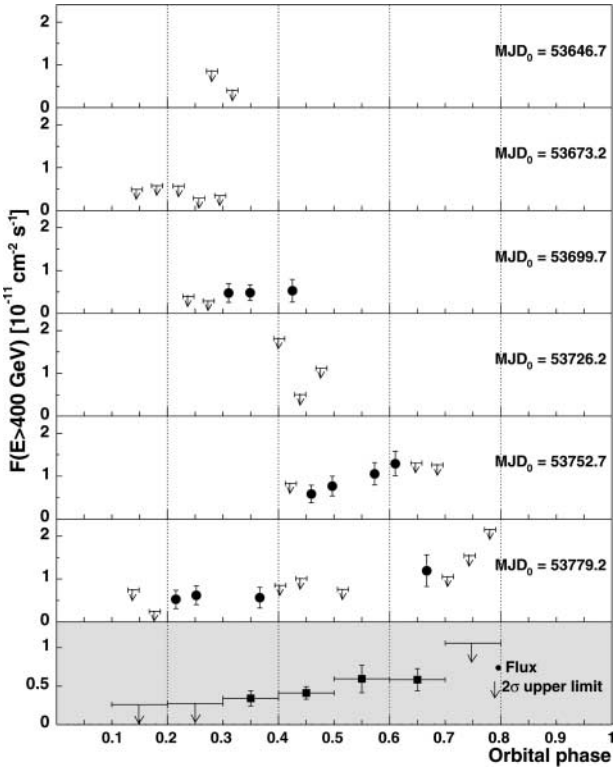

Fig. 2. VHE gamma-ray flux of LS I +61 303 as a function of orbital phase for the six observed orbital cycles (six upper panels, one point per observation night) and averaged for the entire observation time (bottom panel). Vertical error bars include 1σ statistical error and 10% systematic uncertainty on day-to-day relative fluxes. Only data points with more than 2σ significance are shown, and 2σ upper limits (*33*) are derived for the rest. The modified Julian date (MJD) corresponding to orbital phase 0 is indicated for every orbital cycle. The orbital phase is computed with orbital period of 26.4960 days and zero phase at JD 2443366.775 (*9*); periastron takes place at phase 0.23 (*10*). Marginal detections occur between orbital phases 0.2 and 0.4 in different cycles, whereas a significant increase of flux is detected from phase ~0.45 to phase ~0.65 in the fifth cycle, peaking at ~16% of the Crab Nebula flux on MJD 53769 (phase 0.61). During the following cycle, the highest flux is measured on MJD 53797 (phase 0.67). This behavior suggests that the VHE gamma-ray emission from LS I +61 303 has a periodic nature.

The VHE spectrum derived from data between ~200 GeV and ~4 TeV at orbital phases between 0.4 and 0.7 is fitted reasonably well (χ^2/ndf = 6.6/5) by a power-law function: $dN_\gamma/(dA/dt/dE) = (2.7 \pm 0.4 \pm 0.8) \times 10^{-12} E^{(-2.6 \pm 0.2 \pm 0.2)}$ cm^{-2} s^{-1} TeV^{-1}, where $N\gamma$ is the number of gamma rays reaching Earth per

unit area A, time t, and energy E, and E is expressed as TeV. Errors quoted are statistical and systematic, respectively (fig. S2). This spectrum is consistent with that of EGRET for a spectral break between 10 and 100 GeV. We estimate that the flux from LS I +61 303 above 200 GeV corresponds to an isotropic luminosity of $\sim 7 \times 10^{33}$ ergs s^{-1} at a distance of 2 kpc. The intrinsic luminosity of LS I +61 303 at its maximum is higher than that of LS 5039 by a factor of ~6 and is lower than the combined upper limit ($<8.8 \times 10^{-12}$ cm^{-2} s^{-1} above 500 GeV) obtained by Whipple (*23*) by a factor of ~2. LS I +61 303 displays more luminosity at GeV than at x-ray energies, a behavior shared also by LS 5039 (*4*).

Different models have been put forward to explain putative gamma-ray emission from LS I +61 303. Maraschi and Treves (*24*) proposed that the GeV emission measured by COS-B could be due to the wind from a pulsar interacting with that of the stellar companion. However, the detection of radio jets (*16*, *17*) favored an accretion scenario. The observation of jets has also triggered the study of different microquasar gamma-ray emission models. Some of these models are based on hadronic mechanisms: Relativistic protons in the jet interact with nonrelativistic stellar wind ions, producing gamma rays via neutral pion decay (*25*, *26*). Others are based on leptonic mechanisms such as inverse Compton (IC) scattering of relativistic electrons in the jet on stellar and/or synchrotron photons (*27*–*29*).

The TeV flux maximum is detected at phases 0.5 to 0.6 (Fig. 2), overlapping with the x-ray outburst and the onset of the radio outburst. The maximum flux is not detected at periastron, when the accretion rate is expected to be the largest (*30*). This result seems to favor the leptonic over the hadronic models, because the IC efficiency is likely to be higher than that of proton-proton collisions at the relatively large distances from the companion star at this orbital phase. With respect to energetics, a relativistic power on the order of 10^{36} ergs s^{-1} could explain the nonthermal luminosity of the source from radio to VHE gamma rays. This power can be extracted from accretion in a slow inhomogeneous wind along the orbit (*30*).

The variable nature of the TeV emission on time scales of ~1 day constrains the emitting region to be smaller than 10^{15} cm (or ~0.1 arc sec at 2 kpc). This is compatible with the emission being produced within the binary system, where there are large densities of seed photons for IC interaction. Under these strong photon fields, opacity effects certainly play a role in the modulation of the emitted radiation (*31*). Indeed, VHE gamma-ray emission that peaks after periastron passage has been recently predicted with models that consider electromagnetic cascading within the binary system (*32*). In addition, the detection of VHE gamma-ray emission associated with both LS I +61 303 and LS 5039 observationally confirms high-mass microquasars as a population of galactic TeV gamma-ray sources.

LS I +61 303 is an excellent laboratory to study the VHE gamma-ray emission and absorption processes taking place in massive x-ray binaries. The high eccentricity of the binary system provides very different physical conditions to be tested on time scales of less than 1 month.

References and Notes

1. I. F. Mirabel, L. F. Rodríguez, *Annu. Rev. Astron. Astrophys.* **37**, 409 (1999).
2. S. Heinz, R. A. Sunyaev, *Astron. Astrophys.* **390**, 751 (2002).
3. R. C. Hartman *et al.*, *Astrophys. J.* **123** (suppl.), 79 (1999).
4. J. M. Paredes, J. Martí, M. Ribó, M. Massi, *Science* **288**, 2340 (2000).
5. F. Aharonian *et al.*, *Science* **309**, 746 (2005); published online 7 July 2005 (10.1126/science.1113764).
6. D. A. Kniffen *et al.*, *Astrophys. J.* **486**, 126 (1997).
7. D. A. Frail, R. M. Hjellming, *Astron. J.* **101**, 2126 (1991).
8. J. B. Hutchings, D. Crampton, *Pub. Astron. Soc. Pac.* **93**, 486 (1981).
9. P. C. Gregory, *Astrophys. J.* **575**, 427 (2002).
10. J. Casares, I. Ribas, J. M. Paredes, J. Martí, C. Allende Prieto, *Mon. Not. R. Astron. Soc.* **360**, 1105 (2005).
11. P. C. Gregory, A. R. Taylor, *Nature* **272**, 704 (1978).
12. J. M. Paredes, R. Estalella, A. Rius, *Astron. Astrophys.* **232**, 377 (1990).
13. P. Goldoni, S. Mereghetti, *Astron. Astrophys.* **299**, 751 (1995).
14. A. R. Taylor, G. Young, M. Peracaula, H. T. Kenny, P. C. Gregory, *Astron. Astrophys.* **305**, 817 (1996).
15. F. A. Harrison, P. S. Ray, D. A. Leahy, E. B. Waltman, G. G. Pooley, *Astrophys. J.* **528**, 454 (2000).
16. M. Massi, M. Ribó, J. M. Paredes, M. Peracaula, R. Estalella, *Astron. Astrophys.* **376**, 217 (2001).
17. M. Massi *et al.*, *Astron. Astrophys.* **414**, L1 (2004).
18. W. Hermsen *et al.*, *Nature* **269**, 494 (1977).
19. M. Tavani, D. Kniffen, J. R. Mattox, J. M. Paredes, R. Foster, *Astrophys. J.* **497**, L89 (1998).
20. M. Massi, *Astron. Astrophys.* **422**, 267 (2004).
21. J. Albert *et al.*, *Astrophys. J.* **638**, L101 (2006).
22. J. Albert *et al.*, *Astrophys. J.* **637**, L41 (2006).
23. S. J. Fegan *et al.*, *Astrophys. J.* **624**, 638 (2005).
24. L. Maraschi, A. Treves, *Mon. Not. R. Astron. Soc.* **194**, 1P (1981).
25. G. E. Romero, D. F. Torres, M. M. Kaufman Bernadó, I. F. Mirabel, *Astron. Astrophys.* **410**, L1 (2003).
26. G. E. Romero, H. R. Christiansen, M. Orellana, *Astrophys. J.* **632**, 1093 (2005).
27. A. M. Atoyan, F. Aharonian, *Mon. Not. R. Astron. Soc.* **302**, 253 (1999).
28. V. Bosch-Ramon, J. M. Paredes, *Astron. Astrophys.* **425**, 1069 (2004).
29. V. Bosch-Ramon, G. E. Romero, J. M. Paredes, *Astron. Astrophys.* **447**, 263 (2006).
30. J. Martí, J. M. Paredes, *Astron. Astrophys.* **298**, 151 (1995).
31. G. Dubus, *Astron. Astrophys.* **451**, 9 (2006).
32. W. Bednarek, *Mon. Not. R. Astron. Soc.* **368**, 579 (2006).
33. W. A. Rolke, A. M. López, J. Conrad, *Nucl. Instrum. Methods A* **551**, 493 (2005).

34. We thank the Instituto de Astrofísica de Canarias for the excellent working conditions at the Observatory Roque de los Muchachos in La Palma. Supported by the Bundesministerium für Bildung und Forschung and Max-Planck-Gesellschaft (Germany), INFN (Italy), Comisión Interministerial de Ciencia y Tecnología and Ministerio de Educación y Ciencia grant AYA2004-07171-C02-01 (Spain), ETH (Switzerland) research grant TH-34/04-3, and Ministerstwo Nauki i Informatyzacji (Poland) grant 1P03D01028.

Supporting Online Material

www.sciencemag.org/cgi/content/full/1128177/DC1
Figs. S1 and S2

31 March 2006; accepted 8 May 2006
Published online 18 May 2006;
10.1126/science.1128177
Include this information when citing this paper.

The Spiral Structure of the Outer Milky Way in Hydrogen

E. S. Levine,* Leo Blitz, Carl Heiles

We produce a detailed map of the perturbed surface density of neutral hydrogen in the outer Milky Way disk, demonstrating that the Galaxy is a non-axisymmetric multiarmed spiral. Spiral structure in the southern half of the Galaxy can be traced out to at least 25 kiloparsecs, implying a minimum radius for the gas disk. Overdensities in the surface density are coincident with regions of reduced gas thickness. The ratio of the surface density to the local median surface density is relatively constant along an arm. Logarithmic spirals can be fit to the arms with pitch angles of 20° to 25°.

Mapping the Milky Way's spiral structure is traditionally difficult because the Sun is imbedded in the Galactic disk; absorption by dust renders optical methods ineffective at distances larger than a few kpc. Radio lines like the 21-cm hyperfine transition of atomic hydrogen (HI) are not affected by this absorption and are therefore well suited to looking through the disk. The density of HI is roughly proportional to the intensity of the emission, barring optical depth effects. Maps are constructed by using the Doppler shift of the emission line in combination with the rotation structure to determine where in the Galaxy the emission originates. The first maps of the HI density in the midplane of the Milky Way (*1*) made with the use of the 21-cm transition offered the promise that HI mapping of the Galactic plane would reveal its spiral structure by highlighting regions with HI overdensities. The task is easiest outside of the Sun's orbit

Astronomy Department, University of California, 601 Campbell Hall, Berkeley, CA 94720, USA.

*To whom correspondence should be addressed. E-mail: elevine@astron.berkeley.edu